Preferential nucleation of Ge islands at self-organized pits formed during the growth of thin Si buffer layers on Si(110)

J. D. Weil, X. Deng, and M. Krishnamurthy[a)]
Department of Metallurgical and Materials Engineering, Michigan Technological University, Houghton, Michigan 49931

(Received 8 July 1997; accepted for publication 19 September 1997)

The epitaxial growth of thin ($\sim$20–40 nm) Si buffer layer on Si(110) leads to the formation of $\sim$100-nm-wide, uniformly sized faceted pits. The cause of these rhombohedral pits is revealed to be the overgrowth of a homoepitaxial layer over clusters of coherent contaminant particles, possibly SiC. Deposition of Ge on such ''pitted'' surfaces shows highly selective nucleation of pairs of coherent islands at the opposite corners of the pits along the $\langle 110 \rangle$ direction. Continued deposition leads to strain relaxation of one or both of the islands within the pit which then rapidly coarsen to form a single Ge island within the pit. Our observations offer insight into heterogeneous nucleation mechanisms important for producing controlled arrays of self-assembled quantum dots. © *1998 American Institute of Physics.* [S0021-8979(98)00401-0]

I. INTRODUCTION

Coherent islands, formed through deposition of highly lattice-mismatched semiconducting materials, have been observed to have narrow island size distributions,[1] and provide an attractive route for the ''self-assembly'' of quantum dots.[2] More recently, research has focused on techniques that allow for the control of island size, shape, and spatial distribution. Studies conducted on coherent island nucleation have revealed that islands form to partially relieve lattice strain energy at the cost of increased surface energy.[3] However, the mechanisms that dictate the nucleation[4,5] events are not very clear, offering little ability to define predetermined sites for nucleation. While much work has focused on Si(100) and Si(111) surfaces, little literature exists for Si(110) surfaces. Interest in the Si(110) surface stems from the technological advantages over Si(100) in terms of increased electron confinement[6] and the existence of a {111} cleavage plane perpendicular to the (110) surface, allowing easier fabrication of waveguide structures. Fundamentally, the Si(110) surface, due to its surface anisotropy and higher surface energy than Si(100) and Si(111), provides novel insight into the field of silicon heteroepitaxy. We have previously reported on the heterogeneous nucleation of coherent Ge islands on ledges formed during *in situ* oxide desorption on Si(110) surfaces.[7]

In this article, we present the results of a study performed on the epitaxial growth of Ge islands on Si(110) surfaces with thin (20–75 nm thick) Si buffer layers.[8] A high density of uniformly sized ($\sim$100 nm) rhombohedral pits are observed to form subsequent to the growth of the buffer layer. Deposition of Ge on such surfaces leads to nucleation of coherent Ge islands at opposite corners of the pit, forming an island pair or ''dipole''. The islands in the pair have similar sizes at this point. With continued Ge deposition, one of the two islands in the pair grows faster than the other, leading ultimately to the formation of one Ge island at each pit. Our observations are potentially important for the selective nucleation of quantum dots for applications in nanoelectronics.

II. EXPERIMENTAL PROCEDURE

Experiments were performed in a Riber molecular beam epitaxy (MBE) system with base pressure $\sim 5 \times 10^{-10}$ mbar. Si(110) substrates (misoriented to better than $\pm 0.5°$) were rinsed in acetone, methanol, and de-ionized water to remove particle contamination. They were then cleaned in 10% HF solution, followed by a 30:70 oxidation in a solution of H_2O_2:H_2SO_4 and stored in de-ionized water. Prior to loading into the MBE chamber, they were blown dry with nitrogen. After outgassing at 200 °C (until the system approached base pressure), samples were heated to $\sim$925 °C to decompose the oxide layer, following which the surface showed strong diffraction maxima, as indicated by reflection high energy electron diffraction (RHEED). The samples were then cooled to the Si buffer-growth temperature, $\sim$500 °C, at which point the RHEED pattern indicated a (16×2) surface reconstruction pattern, consistent with a clean Si(110) surface.[9,10] Si buffer layers were deposited from a compact electron beam Si source calibrated at $\sim$0.3 nm/min. After every 10–15 nm of the Si buffer growth, deposition was halted and the sample was heated to $\sim$800 °C and held at this temperature for about 3–5 min, then cooled to the Si growth temperature. The total annealing times (including heating and cooling) was $\sim$10 min. This procedure helped ensure a high-quality buffer layer as evidenced from a sharper RHEED pattern. Ge was deposited on the buffer layer from a pyrolitic boron nitride Knudsen source previously calibrated to have a rate of $\sim$0.9 nm/min. The Ge deposition was conducted 10 s at a time, followed by careful scanning of the surface with RHEED. All Ge deposition was performed at a substrate temperature of 700 °C ($\pm$25 °C) with $\sim$0.6 nm (40 s) total coverage. The only parameter varied was the buffer layer thickness, between 30 and 75 nm. One sample (called sample X), had slightly different surface preparation conditions. The sample was not introduced to either acetone or methanol during the sample

a)Electronic mail: mohan@mtu.edu

 0021-8979/98/83(1)/212/5/$15.00

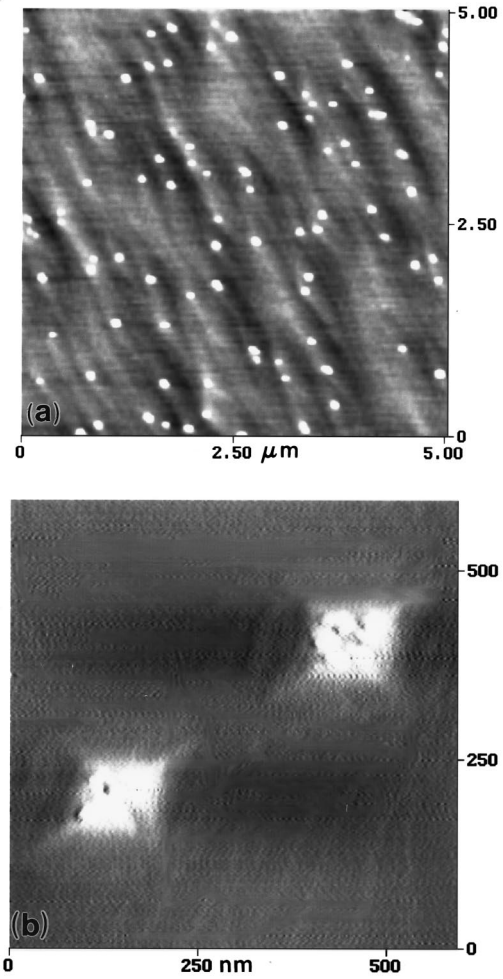

FIG. 1. AFM image of a Si(110) surface after the *in situ* oxide desorption, showing (a) high density of contaminant clusters and ripples (step bunches) along ⟨111⟩ directions and (b) magnified view of the clusters of smaller (SiC) particles.

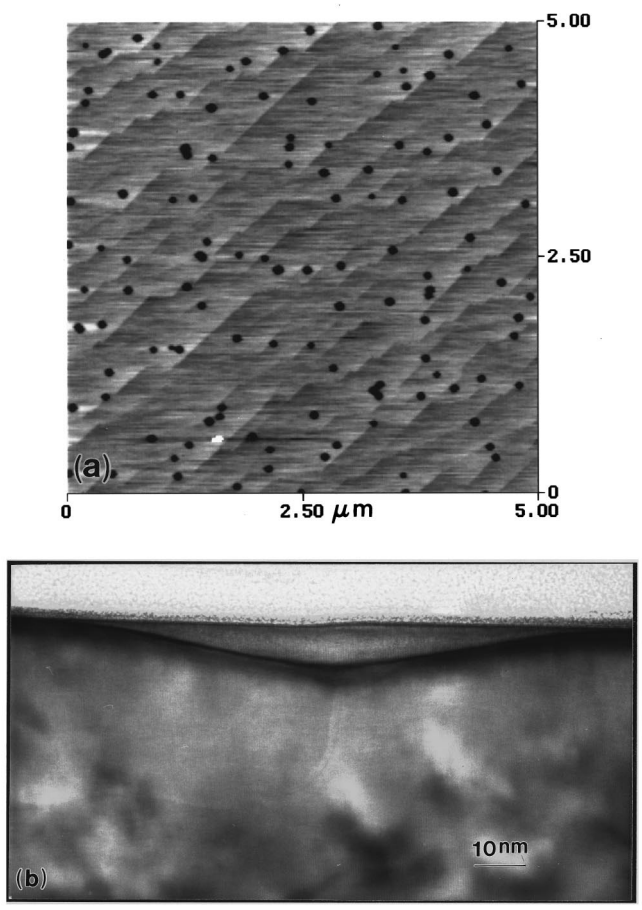

FIG. 2. Surface morphology after the growth of a 20 nm Si buffer layer on Si(110). (a) AFM image showing uniform sized rhombohedral pits and ⟨111⟩ oriented ledges. (b) Cross-sectional TEM image showing a faceted pit.

preparation stages. Second, the buffer layer for this sample was grown at 700 °C, as opposed to 500 °C for all other growths. All samples were analyzed *ex situ* using atomic force microscopy (AFM) (Nanoscope IIIa) and plan-view and cross-sectional transmission electron microscopy (TEM), using JEOL 100cx and 4000fx microscopes.

III. RESULTS

Figure 1(a) shows an AFM image of a Si(110) surface after the oxide desorption process. Surface waves (roughness) on the order of ~ 2 nm as well as small islands are observed. Magnified views of these islands shown in Fig. 1(b) indicate that these islands are actually clusters of much smaller contaminant particles, possibly SiC.[11] These particles are typically <50 nm in diameter and <10 nm in height and each cluster consists of 2–6 particles. The surface waves appear to be ⟨111⟩ oriented step bunches (ledges) formed possibly from pinning of surface steps by the contaminant clusters. While the average density of clusters is roughly 4×10^8 cm^{-2}, there are slight variations within the wafer and from wafer to wafer.

After the deposition of a 20 nm Si buffer layer, the formation of uniform-sized rhombohedral pits can be seen, as shown in Fig. 2(a). The number density of pits ($\sim 4 \times 10^8$ cm^{-2}) and their shape suggests that their formation is likely to be associated with the contaminant particles. The pits observed here are typically 100 nm wide. A section analysis shows that the faceted walls of the pit make $\sim 8° - 11°$ angle with the substrate, as also confirmed by the cross-sectional transmission electron microscopy (XTEM) image of a pit (taken along a ⟨112⟩ zone) shown in Fig. 2(b). This facet angle is very typical of the pits examined on this surface. The other features of interest in Fig. 2(a) are the ledges formed along crystallographic ⟨111⟩ directions. The height of these ledges is typically ~ 1 nm and the width is ~ 60 nm.

Figure 3(a) shows the surface morphology of sample X (the one with a slightly different cleaning procedure and buffer growth at 700 °C) after the 0.6 nm Ge deposition. First, the average density of pits on this sample is $\sim 1 \times 10^9$ cm^{-2}, almost twice that of the surface in Fig. 2(a). The average size of pits is ~ 200 nm on a side, with the pit walls making 8°–11° facets, similar to that observed in the other samples. A few of these pits have large Ge islands in them. Most of the other pits have pairs of small islands that have nucleated at the opposite corners of the pit. The orien-

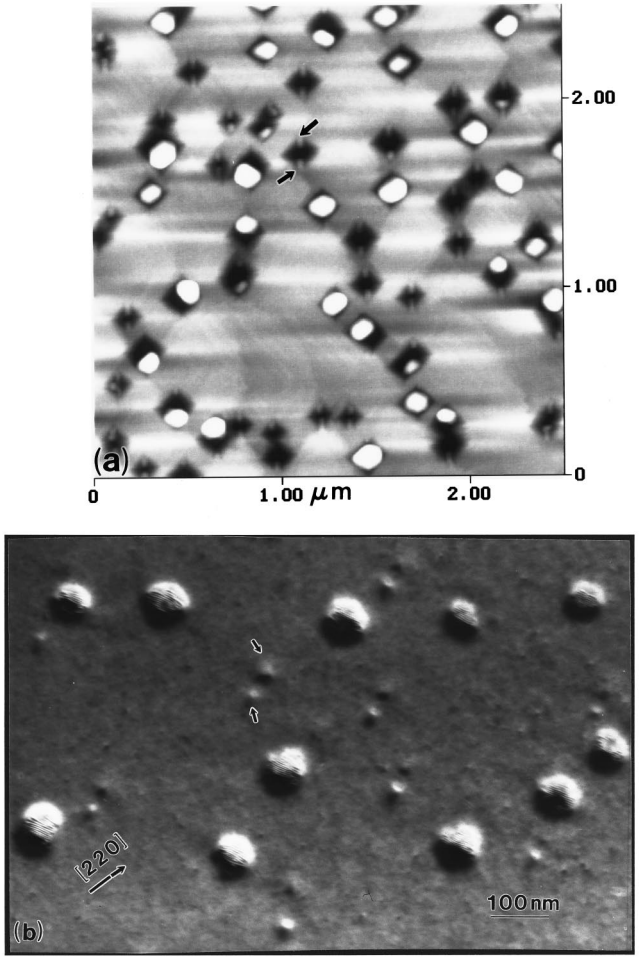

FIG. 3. Surface morphology after 0.6 nm Ge has been deposited on a 20 nm Si buffer. (a) AFM image showing a high density of pairs of islands (dipoles) formed at two opposite corners of the pit. (b) Plan-view TEM image showing that these dipoles are oriented along ⟨100⟩ and are coherent.

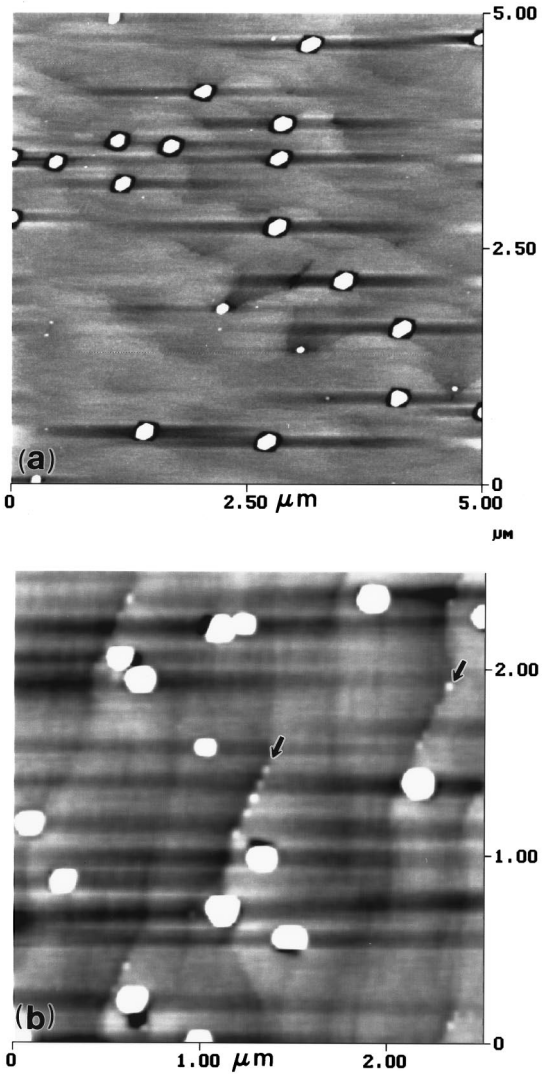

FIG. 4. AFM image showing Ge island nucleation at various heterogeneous sites. (a) Highly selective nucleation of Ge islands at a pit and (b) Ge islands at ledges and surface pits. Two ledges are indicated with arrows.

tation of the island pair (dipole) is consistently along the lone ⟨110⟩ direction. It is seen in some images that islands may start to form at the other two corners of the pit, forming an interesting island ''quadrupole'' cluster. The plan-view TEM image shown in Fig. 3(b) confirms not only the orientation of the island pairs, but also the fact that these dipole islands are coherent, revealing that coherent islands initially form at the corners of pits.[8]

Figure 4(a) is an AFM image of a surface with 0.6 nm Ge coverage. Notice that all islands are confined to pits. TEM images show that such islands have typically relaxed their strain by forming interfacial dislocations. Interestingly, the dislocated islands find it more favorable to fill the area of the pit, rather than grow vertically. Figure 4(b) is an image of a surface with 0.6 nm Ge coverage, emphasizing the nucleation of Ge islands along ledges. All the islands are less than 3 nm tall, between 40 and 60 nm in diameter, and evenly spaced ~80 nm apart. The ledge on which these islands are located is ~60 nm wide, ~1.5 nm tall, and makes an angle ~1.5° with the substrate. These ledges are likely to have formed during the deposition of the buffer layer [Fig. 2(a)]. The island density on this sample is slightly lower than the average and indicates that with a lower pit density, island nucleation at ledges becomes more prominent.

With thick enough buffer layers, pits eventually fill in, resulting in a smooth layer. Figure 5 shows an area of a sample on which a ~75 nm buffer layer of silicon was deposited, followed by 0.6 nm of Ge at 700 °C. It can be seen that the density of islands ($\sim 10^8/\mathrm{cm}^2$) is lower than the density of pits observed on the buffer layers shown in Figs. 2 or 3. Smaller individual islands and a few large islands are observed, but pits can only be resolved adjacent to the largest islands. It is therefore suggested that the much thicker buffer layer of this sample has completely covered most of the pits in this region and the smaller islands that have nucleated randomly are likely to be coherent.

IV. DISCUSSION

The origin of the uniformly sized pits and the nucleation of Ge islands need to be discussed. We begin by suggesting that the as-cleaned (after complete *in situ* oxide desorption)

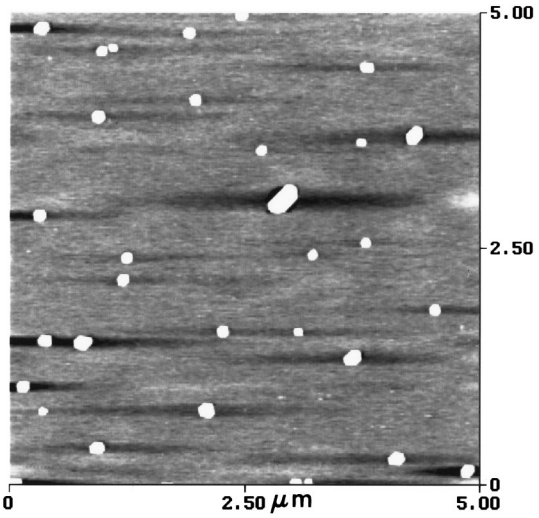

FIG. 5. AFM image of Ge nucleation on a relatively pit-free surface showing random distribution of Ge islands. A few islands may still be influenced by heterogeneous nucleation sites.

Si substrate (shown in Fig. 1) consists of SiC contaminant particles and surface roughness in the form of step bunches pinned by these particles. The formation of step bunches is not surprising given the instability of the Si(110) surface relative to (111) or (100) surfaces and the possibility of unintentional local surface misorientation. The morphology of the clusters suggests that a single SiC precipitate may have split into several smaller precipitates due to strain effects.

The observation that the contaminant cluster density on the clean Si surface correlates with the pit density of the Si buffer layer suggests that the overgrowth on the contaminant particles causes pit formation. A similar observation has been used to describe the ''pagoda'' defect[12] and is ascribed to a low sticking coefficient of Si on SiC contaminant particles. In addition, it has been suggested that SiC particles may exist as coherent or incoherent precipitates on the substrate surface.[13] While the coherent SiC precipitates locally strain the surrounding Si matrix, incoherent carbides, on the other hand, will form threading dislocations that extend through the buffer layer. Based on our TEM observations, we believe that the clusters of SiC particles in our experiments are mostly coherent with the Si substrate. Consequently, the following model of thin Si buffer growth can be inferred. Due to the large lattice mismatch and difference in surface energy between Si and the SiC particulates, arriving Si adatoms find the contaminant areas energetically unfavorable for incorporation. Consequently, continued deposition results in the formation of pits (with stable facets) over the contaminant clusters. It is possible that the increase in surface energy associated with the facets may accommodate strain energy due to heteroepitaxy of Si on SiC. With increasing buffer layer thickness, the strain energy per unit volume in the Si epilayer decreases. At some critical epilayer thickness, the excess surface energy associated with the pit walls will become larger than that required for strain relaxation, i.e., less surface energy is required to offset the decreased strain energy. Subsequently, the pit gradually fills in,

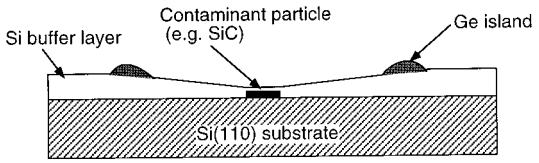

FIG. 6. Schematic figure showing a faceted pit and the nucleation of a Ge island dipole.

leading to a flat buffer layer, with some residual strain centers located over the buried contaminants.

When Ge adatoms are deposited on the pitted surface, the adatoms seek energetically favorable sites for attachment. The corner location of the pit serves as a low nucleation-barrier heterogeneous site for Ge island growth. The preferential nucleation at the two opposite corners of the pit (along the ⟨110⟩ diagonal of the pits) is possibly related to the fact that by doing so, the free surface of the islands can fully relax into the pit, in the elastically harder direction and elastically deform along the one elastically soft ⟨100⟩ direction. Within the constraints of the pits, these two corners may offer the lowest energy island configuration, as shown schematically in Fig. 6. The uniformity of island sizes within the pits suggests that the islands effectively ''communicate'' by surface diffusion, leading to a uniform growth rate. Furthermore, if the density of pits is high enough, diffusion of Ge adatoms between pits will allow the growth of an assembly of uniform sized coherent island dipoles, as observed in Fig. 3. Continued growth leads to further relaxation (by dislocation formation) of one of the two islands within the pit, which then grows rapidly at the expense of the other island. This would then lead to the formation of a large relaxed island at each pit, as evident, for example, in Fig. 4(a). When the pit density is lower, nucleation may also occur at the ledges, as seen in Fig. 4(b).

If Ge is deposited on a thicker (and apparently flat) buffer layer (e.g., Fig. 5), islands appear to nucleate randomly and pits can only be resolved near a few of the individual islands. In addition, the presence of a few island dipoles suggests that preferential nucleation may still occur when pits are overgrown. It is suggested that the strain field over coherent contaminant particles or residual roughness near pits can still influence nucleation of Ge islands on an apparently flat surface. Similar effects of buried contaminants have been reported for the growth of SiGe alloys on Si surfaces.[14]

In conclusion, our studies on the initial stages of Ge growth on thin Si buffer layers on Si(110) demonstrate that faceted pits form during the deposition of a thin Si buffer layer. The cause of these pits is revealed to be overgrowth of a homoepitaxial layer over clusters of coherent contaminant particles. Deposition of Ge leads to preferential nucleation of pairs of coherent islands ordered along the elastically soft ⟨100⟩ direction. Continued deposition leads to strain relaxation of one or both of the islands within the pit which then rapidly coarsens to form a single Ge island in each pit. Our observations offer insight into preferred heterogeneous nucleation sites, which may be important for producing controlled arrays of self-assembled quantum dots.

ACKNOWLEDGMENTS

The authors would like to thank Joe McLaughlin for help with TEM sample preparation and gratefully acknowledge financial support from NSF-DMR (9624456) and a DARPA-ULTRA Nanoelectronics grant through AFOSR (F-49620-96-1-0313).

[1] M. Krishnamurthy, J. S. Drucker, and J. A. Venables, J. Appl. Phys. **69**, 6461 (1991).
[2] D. Leonard, M. Krishnamurthy, C. M. Reaves, S. P. DenBaars, and P. M. Petroff, Appl. Phys. Lett. **63**, 3203 (1993); J. M. Moison, F. Houzay, F. Barthe, L. Leprince, E. Andre, and O. Vatel, *ibid.* **64**, 196 (1994).
[3] D. J. Eaglesham and M. Cerullo, Phys. Rev. Lett. **64**, 1943 (1990); S. Guha, A. Madhukar, and K. C. Rajkumar, Appl. Phys. Lett. **57**, 2110 (1990).
[4] J. Tersoff and F. K. LeGoues, Phys. Rev. Lett. **72**, 3570 (1994).
[5] See, for example, D. E. Jesson, K. M. Chen, S. J. Pennycook, T. Thundat, and R. J. Warmack, Phys. Rev. Lett. **77**, 1330 (1996) and references therein.
[6] C. W. Liu, J. C. Sturm, Y. R. J. Lacroix, M. L. W. Thewalt, and D. D. Perovic, Appl. Phys. Lett. **65**, 76 (1994).
[7] M. Krishnamurthy, B.-K. Yang, and C. G. Slough, Appl. Phys. Lett. **70**, 50 (1997).
[8] J. D. Weil, B.-K. Yang, and M. Krishnamurthy, Mater. Res. Soc. Symp. Proc. **440** (1996).
[9] Y. Yamamoto, S. Ino, and T. Ichikawa, Jpn. J. Appl. Phys., Part 1 **25**, L331 (1986).
[10] H. Kim, N. Taylor, T. Spila, G. Glass, S. Y. Park, J. E. Greene, and J. R. Abelson, Surf. Sci. **380**, L496 (1997); Y. Yamamoto, T. Sueyoshi, T. Sato, and M. Iwatsuki, J. Appl. Phys. **75**, 2421 (1994).
[11] A low density of carbide particles is commonly seen after high temperature Si clean. See, for example, J. S. Drucker, M. Krishnamurthy, and G. G. Hembree, Ultramicroscopy **35**, 323 (1991) and references 9, 10, and 13 within; D. J. Eaglesham, G. S. Higashi, and M. Cerullo, Appl. Phys. Lett. **59**, 685 (1991).
[12] M. Dynna, D. D. Perovic, and G. C. Weatherly, Philos. Mag. A **66**, 375 (1992).
[13] D. D. Perovic and G. C. Weatherly, Thin Solid Films **183**, 141 (1989).
[14] K. M. Chen, D. E. Jesson, S. J. Pennycook, T. Thundat, and R. J. Warmack, Appl. Phys. Lett. **66**, 34 (1995).